PNAS
www.pnas.org

Temporal Changes Guided by Mesenchymal Stem Cells on a 3D Microgel Platform Enhance Angiogenesis In Vivo at a Low-Cell Dose

Dilip Thomas[1,2]*, Grazia Marsico[1], Isma Liza Mohd Isa[1], Arun Thirumaran[2], Xizhe Chen[2], Bartlomiej Lukasz[3], Gianluca Fontana[1], Brian Rodriguez[3], Martina Marchetti-Deschmann[4], Timothy O'Brien[1,2], Abhay Pandit[1]*

*Prof. Abhay Pandit,
Email: abhay.pandit@nuigalway.ie
*Dr. Dilip Thomas
Email: dilip.thomas@outlook.com

This PDF file includes:

www.pnas.org/cgi/doi/10.1073/pnas.2008245117

Supplementary Information

SI Materials and Methods

Culture of Cells

hMSC primary cells were isolated from fresh human bone marrow. Cells were isolated in the same media as used during the passaging, so the cells were never exposed to more than one type of serum. Non-adherent cells were removed after three days, after which the media was changed twice per week. Isolated cells were characterized based on the routine tri-lineage differentiation potential and the presence of cell surface markers using flow cytometry. hMSCs were cultured in complete medium (MEM alpha, GlutaMAX™ supplemented with 10% fetal bovine serum and 1% penicillin/streptomycin) and maintained at 37°C in a humidified atmosphere containing 5% CO_2. For both *in vitro* and *in vivo* experiments MSCs were pooled from four to six unrelated bone marrow donors, and after routine characterization and were frozen down at passage P1.

Assessment of Cell Morphology

Microgels were imaged for four days' post-fabrication for changes in cell morphology. Microgels were briefly washed in phosphate-buffered saline (PBS) and incubated with 10mM calcein AM (Fluka, Germany) for ten minutes. Samples were then imaged as Z-Stacks through 500-800μm on an Andor™ Olympus Spinning Disk Microscope (Andor, Belfast, Northern Ireland), using Andor™ IQ software, with an 20X oil immersion objective lens. Green viable cells were visualized by excitation with the 488nm laser line. Sample images were obtained as Z-slices 5μm apart. Each Z-stack was analyzed using the Volocity® 5.0 software (Perkin Elmer Inc., Waltham, USA). Cell morphology parameters such as shape factor index, surface area-to-volume ratio and longest cell axis distance were analyzed. Shape factor is the ratio of surface area of a sphere to the surface area of the object. In the equation below A_0 is the surface area and V_0 is the volume.

$$\text{3D Shape Factor} = \frac{\pi^{\frac{1}{3}}(6V_0)^{\frac{2}{3}}}{A_0}$$

Datasets were analyzed using defined algorithms to estimate a series of measurements related to the dynamic changes in cell morphology across three different planes (top, middle and bottom) of the microgels.

Assessment of Changes in Microgel Modulus Seeded with hMSCs

For measuring the Young's modulus of the cell seeded microgels incubated for 24 or 96 h, atomic force microscopy was utilized. All the measurements were performed with MFP-3D-BIO AFM (Asylum Research/Oxford Instruments, US) fitted on a Ti/E inverted microscope (Nikon, Japan) and run with Igor Pro™ 6.34A software (WaveMetrics, US) with Asylum Research plugin (ver. 120804+2209). Probes were prepared by fixing 10μm silica glass spheres (Windsor Scientific, UK) at the end of type B CSC38 tipless AFM cantilevers (Mikromasch, Bulgaria) with epoxy glue. Stiffness and sensitivity of the cantilevers were calibrated in air (Sader, non-contact method) and subsequently in PBS (contact method) to correct for changes in lever sensitivity. These values ranged between 62.25 and 83.25nm/V for sensitivity (in liquid), and between 64.7 and 73.15pN/nm for lever spring constant.

Microgels suspended in PBS were deposited on a microscope glass slide and allowed to settle down for ten minutes. This sample preparation appeared to prevent the microgel from rolling during indentation; however, movement of the microgel or rolling of the spherical tip on the surface could lead to errors in quantification of the modulus. For each condition, namely microgels prepared with 1, 2 or 3 $mg \cdot mL^{-1}$ collagen which were seeded with cells (following 24 or 96 h incubation and fixing with alcohol), 3-4 microgels were chosen and 36-68 measurements were performed per group (4-29 per microgel). Each measurement consisted of an indentation with constant a loading force of 100pN, 3-5μm force distance and 1μm/s tip approach/retraction speed. Used force was optimized to avoid indentation depths greater than 3μm (30% of the silica sphere tip) on the softest sample. The measurements on the microgels were performed in liquid, and the resulting force-distance curves were processed with Asylum plugin for Igor using a Hertz model (1).

Indenter (silica sphere) modulus was assumed as 68.00GPa and its Poisson's ratio was assumed as 0.19. Considering the viscoelastic properties of a swollen hydrogel, its Poisson's ratio was set to 0.5 (2). The whole curve length was used for fitting, except in the cases where good fit quality could only be achieved by fitting only the contact portion. Fit quality was assessed with a reduced chi square value (χ^2) calculated for each modulus and was further used to obtain a weighted average modulus for a given sample type. The closer χ^2 was to 1, the better the fit.

Analysis of Cell Viability

Microgels were then digested in collagenases for 20 minutes and sterile filtered with 70μm filter mesh to harvest cells. Before analysis on BD FACS Canto (BD Biosciences, USA), cells were re-suspended in propidium iodide/RNase staining buffer (BD Biosciences, Ireland). Live cells (PI-negative) and dead cells (PI-positive) cells were included for analysis using FlowJo software 8.5.2 (Tree Star, Ashland, OR).

Scanning Electron Microscopy (SEM) Imaging of hMSC Embedded Microgel

Microgels were washed with PBS twice and fixed in 2.5% glutaraldehyde for three hours. Then, the samples were dehydrated in a graded ethanol series and air-dried. After gold sputtering, the microgels were examined with a Hitachi S-4700 scanning electron microscope (Hitachi Scientific Ltd., Japan).

Ultrastructure Analysis of Cellular Inclusions

Microgels were fixed for four hours at room temperature in 2.5% glutaraldehyde at pH 7.4, post-fixed in 1% osmium tetroxide in 0.2M sodium cacodylate buffer at pH 7.4 for one hour. The microgels were dehydrated in a series of graded ethanols and infiltrated with a mixture of propylene oxide and epoxy resin (Agar Low Viscosity Resin kit, Agar Scientific, UK), and finally infiltrated with 100% resin on a rocker overnight. The microgel embedded resin blocks were then cured in an oven at 65°C for 48 h. Ultrathin sections were cut and transferred to standard transmission electron microscope (TEM) grids and contrasted with uranyl acetate before being viewed under TEM for imaging. TEM images of the cell embedded microgels were transformed to an 8-bit image (Fiji-ImageJ software) (3). Subsequently, a classifier plugin was trained on the TEM micrographs using Trainable Weka Segmentation plugin, defining dark cellular inclusions and all other intracellular organelles (background). The total cell area and the number of cellular inclusions were quantified using automated threshold of the respective probability map image and object counter analysis of Fiji/ImageJ with an average inclusion size less than 500μm^2.

Cell Surface Marker Analysis of hMSCs

Flow cytometry analysis was used for confirming the presence of human mesenchymal stem cell surface markers. The cells were harvested by collagenase digestion of microgels and washed twice in PBS. The cells were re-suspended in FACS buffer (PBS, 2% FBS and 0.1% NaN3). Approximately, 5-7 × 10^4 cells were incubated with anti-human primary monoclonal antibodies CD90, CD105, CD73, CD45, CD34, CD14, and CD20 (Miltenyi Biotec, Bergisch-Gladbach, Germany). Data was acquired by BD FACS Canto (BD Biosciences, San Jose, CA) FACS Calibur flow cytometer and analyzed by FlowJo software (TreeStar Inc., OR, USA).

Immunostaining for $\alpha V\beta_3$ and Vitronectin

Microgels cultured for 96 h were fixed in 4% paraformaldehyde for 30 minutes and blocked with 10% normal goat serum for two hours. Microgels were then incubated with mouse anti-human $\alpha V\beta_3$ (Santa Cruz Biotechnology) and rabbit anti-human Vitronectin (Santa Cruz Biotechnology) primary antibody (1:200) in 2% goat serum overnight at 4°C. Alexafluor® 488, goat anti-mouse IgG (1:100) and Alexafluor® 594, goat anti-rabbit IgG (1:100) secondary antibody was incubated for one hour at room temperature in blocking buffer. Following six PBS washes, nuclei were counterstained with Hoechst (Life Technologies) for five minutes. Samples were then imaged as Z-Stacks on Andor™ Olympus Spinning Disk Microscope (Andor, Belfast, Northern Ireland), using Andor™ IQ software, with an X 20 objective lens. Calculation of protein expression and Pearson's co-localization coefficients were calculated in Volocity® 5.0 software (Perkin Elmer Inc., Waltham).

Histology and Immunohistochemistry
Three weeks after the treatment mice were sacrificed to harvest the tissue. Hindlimb gastrocnemius and lower quadriceps muscles were carefully dissected and weighed before being fixed in 4% PFA for 48 h. The samples were then rinsed with PBS before being snap frozen followed by embedding in Optimal Cutting Temperature (OCT) compound (TISSUE-TEK®; Sakura Finetek USA. Inc.). Cryosections were taken at a thickness of 7µm from four different depths at 50µm intervals using a Leica CM1850 cryostat (Leica Microsystems, Germany) set at -22°C. The samples were stained with hematoxylin and eosin (H&E). For immunofluorescence, cryosections were treated with 1X proteinase K solution and incubated at 37°C for 20 minutes for antigen retrieval. The tissue sections were blocked with 1% BSA for two hours to avoid non-specific binding. Anti-mouse polyclonal primary antibody specific for CD31/PECAM-1 (Abcam, Ireland) endothelial marker or CD68 (Abcam, Ireland) macrophage marker were incubated overnight at 4°C. Secondary antibody labelled with AlexaFluor® 488 or AlexaFluor® 594 (1:500, Invitrogen, Ireland) was applied for one hour at room temperature, followed by nuclear counter staining using Hoechst dye (Life Technologies).

Lectin Histochemistry
For lectin histochemistry, the muscle sections were washed two times with distilled water for five minutes each. Slides were washed with Tris-Buffered Saline (TBS) 1X enriched with $Ca2^{+}$ and $Mg2^{+}$ cations (20 mM Tris-HCl, 100 mM NaCl, 1 mM CaCl2, 1 mM MgCl2, pH 7.2) and then blocked with 2% periodate-treated bovine serum albumin in TBS for one hour. Sections were then incubated with either Wheat germ agglutinin (WGA) (10µg/ml) or Ulex Europaeus Agglutinin I (UEA-1) (15µg/ml) lectin labelled with fluorescein isothiocyanate (FITC) (EY Labs Inc.) in TBS for one hour. The sections were washed three times with TBS and nucleus was counterstained with DAPI (1:10000). All slides were cured in dark overnight prior to imaging on an Andor™ Olympus Spinning Disk Microscope (Andor, Belfast, Northern Ireland).

Model of Hindlimb Ischemia
All the animal treatment groups and experimental procedures were approved by the institutional Ethics Committee. A recently developed double ligation hindlimb ischemia nude mouse model (4)was used to test the therapeutic efficacy of the optimized 2-mg·mL^{-1} and 0.8 million cells microgel construct. The mice were anesthetized with intra-peritoneal injections of xylazine (10 mg/kg) and ketamine (80 mg/kg). For hindlimb ischemia induction, two separate skin incisions were made; one around the groin area and the other above the knee. The artery was then carefully separated from the vein and a ligation was placed before the profunda femoris. This was followed by a second ligation placed before the saphenous–popliteal bifurcation branch. A cut was then made between the ligation sites interrupting the blood flow to the limb. Mice were divided into the following treatment groups (n=12/group): hMSC embedded microgels (30±5, 1600 cells/microgel), $5x10^4$ cells (low-cell density; approximately the same number of cells embedded in microgels), $1x10^6$ cells (high-cell density), microgels alone and saline which were implanted or injected at the proximal artery ligation site after surgical induction. The incision was then sutured closed and the animals were given analgesic of 0.05mg/kg buprenorphine prior to recovery from anaesthesia. Laser Doppler measurement was acquired weekly for three weeks, along with the assessment for improvement in ambulation and signs of necrosis or auto-amputation. The animals were sacrificed at the end of the three weeks to harvest the tissue.

Assessment of Ambulation and Necrosis
The efficacy of the treatment was evaluated semi-quantitatively by gross examination of the foot. Limb condition was classified into several levels of severity and scored based on signs of necrosis and the extent of plantar flexion or dragging observed on the operated foot while walking. A point-based scale was devised to quantify the extent of necrosis in the limb with 0=blue correlated with no necrosis to 5=black indicative of severe necrosis. Similarly, ambulatory impairment was graded between 0 and 3, where 0 refers to normal ambulatory function similar to the non-operated foot and 3 indicates poor ambulation manifested by dragging of the foot. Two blinded independent scorers carried out the scoring every week for three weeks.

Histomorphometry
Histomorphometric analyses is typically performed to quantify tissue responses to injectable or implantable therapeutics. It allows assessment of angiogenesis in vascular beds and infiltration of inflammatory cells(5). In order to avoid observational bias in sampling, a systematic methodology was employed throughout the study as previously described(5-9). For quantification of the blood vessels and infiltration of inflammatory cells, twenty images per sample per animal were analyzed across four levels separated by 50µm. The 'forbidden line' method was used to count the blood vessels that run parallel depending on how the vessel intersects or does not intersect in the counting frame(10). This quantification is robust and highly representative of the changes that occur in tissues. In the current study 70-80 tissue sections per animal in each group were analyzed.
The fields were captured at 40X magnification. A grid mask with squares of defined dimensions was placed on the histology sections using Image Pro® Plus software. Quantified parameters were capillary density, radial diffusion and the area fraction of infiltrating inflammatory cells.

Vessel Density and Radial Diffusion
For angiogenesis, the points where the squares on the grid intersected blood vessels were numbered on the section. The surface capillary density of blood vessels was calculated using the intersected blood vessels multiplied by the area of the total area of the tissue within the square. Radial diffusion was calculated using the formula (1/SQRT(L_v*PI)*1000, which is the distance between blood vessels and is an indicator of the capillary network in the vascular bed. The shorter the distance between blood vessels, the smaller the distance required for nutrients to diffuse into surrounding tissues.

Area Fraction of Inflammatory Cells
The area fraction of infiltrating inflammatory cells was also evaluated. Inflammatory cells were counted and these cells included lymphocytes and neutrophils. The area fraction was determined with a 1938 points grid using Image Pro® Plus software (Media Cybernetics). Neutrophils were identified as small dense circular multi-lobed cells and lymphocytes as small round dense cells with large nuclei.

Tissue RNA Extraction and Mouse Endothelial PCR Arrays
RNA from muscle tissues was stored in RNAlater® (Thermo Fisher Scientific, UK) and extracted using RNAeasy® Microarray Tissue mini kit (Qiagen GmbH, Germany). Tissues were homogenized using TissueLyser LT(Qiagen) for 20 minutes at 50Hz. Extracted RNA samples were treated with DNase to remove contaminating genomic DNA. RNA quality was assessed using the Agilent 2100 Bioanalyzer (Agilent Technologies, CA) and samples with RNA Intergrity Number (RIN) RIN >7 were used for downstream cDNA conversion with a RT^2 first-strand kit (Qiagen GmbH, Germany) according to the manufacturer's protocol. Eighty-four gene targets were analyzed on a Mouse Endothelial Cell Biology RT^2 profiler PCR array (PAMM-015Z, SaBiosciences Corp., USA). Statistical analysis of relative gene expression results in real-time PCR was performed using REST© software tool (11). Briefly, a Pair-Wise Fixed Reallocation Randomization Test was used to determine significant differences between the treatment and the control groups (n=3/treatment group; n=1 pooled tissue samples from four animals). A *P*-value less than 0.05 was considered to be significant.

Ingenuity Pathway Analysis
The genes for *in vitro* and *in vivo* PCR-arrays were uploaded to Ingenuity Pathway Analysis (IPA) software. Pathway analysis was performed from information contained in the IPA knowledge base (IPKB). The database was limited to human, mouse and rat species. For network analysis, IPA computed a score (p-score=-log10(*P*-value)) according to the fit of the set of supplied genes and a list of biological functions in IPA. The score considers the number of genes in the network and the size of the network to approximate how relevant this network is to the original list of genes and allows the networks to be prioritized for further studies. A z score ≥2 (or ≤−2) (*P* <0.05) was considered significantly activated or inhibited.

Tissue Sample Processing and MALDI Mass Spectrometry Imaging for *N*-Glycans

Unfixed muscle tissue samples from the upper gastrocnemius were stored at -80°C for mass spectrometry imaging (MSI) and MALDI-TOF analysis after in-solution glycan release. For MSI experiments and H&E staining, consecutive cryosections of 15µm in OCT were cut using Leica CM3050 (Leica Microsystems, Germany) and thaw-mounted on conductive indium tin oxide (ITO)-coated glass slides (Delta technologies, USA). Frozen tissues were thawed and dried in a vacuum desiccator for one hour at room temperature before washing. Tissue sections were washed in double distilled water (ddH_2O) and sequentially dehydrated in graded ethanol solution (50-100%) for 30 seconds each. Dehydrated sections were washed in NH_4HCO_3 (10mM, pH 8.0) twice for five minutes and air dried at room temperature. Glycerol-free PNGase F (200 µl) (New England Biolabs, UK) was dialysed in NH_4HCO_3 (25mM, pH 8.0) and applied on tissue (15nL at 100 µm spacing) using a ChIP-1000 (Shimadzu, Japan). No-enzyme controls were printed using the NH_4HCO_3 buffer. Tissue sections were incubated overnight at 37°C in a humidified chamber, and a defined peptide mix was spotted adjacent to the section for TOF calibration. 2,5-Dihydroxybenzoic acid (DHB) matrix (5.5 $mg \cdot mL^{-1}$) in 0.1% TFA containing 1 mM NaCl was deposited on the specimens using a home-built sublimation apparatus (Marchetti-Deschmann laboratory, TU Wien), and recrystallization of the matrix was performed by hydrating the slides in vapours of acetic acid in a humidified chamber (12). MSI data was acquired on a MALDI TOF/TOF (ultrafleXtreme™, Bruker Daltonics, Germany) mass spectrometer in reflectron mode (using a spatial resolution of 50 µm and 50 shots per position of a random walk within each pixel) with glycan masses ranging up to *m/z* of 2500. Flex Imaging™ v3.0 (Bruker Daltonics, Germany) was used for data and image processing. All presented images are total ion current (TIC) normalized.

In-solution Tissue Digest for *N*-Glycan Release

Muscle tissue chunks from the upper gastrocnemius were microdissected and placed in eppendorfs for washing. Tissues were washed once with ultra-high-quality water (ddH_2O) with an additional two washes (2 x 5 minutes) with 10mM NH_4HCO_3. The tissues were incubated in 10mM NH_4HCO_3 at 95°C for 30 minutes. Further, tissues were gently homogenized with tweezers in the eppendorf tube and centrifuged at 8,000RPM for ten minutes. The supernatant tissue lysate was incubated with glycerol-free PNGase F at 37°C overnight. The mixture was deposited onto a ZipTip C18 tip, and glycans (together with unbound proteins/peptides) were obtained in the flow through and spotted with DHB matrix onto an MTP-384 AnchorChip™ target (Bruker Daltonics) and allowed to dry at room temperature. For calibration, a standard peptide mix was spotted separately onto calibrant AnchorChip spots. MS data was obtained on the same instrument described above using FlexControl™ v.3.4 (Bruker Daltonics). For analysis, automatic peak picking was performed using a signal-to-noise (*S/N*) threshold of 7. Peak identity and intensities of *m/z* values were matched with MSI experiments for the same sample and represented as ion intensity maps on the tissues. The target parent ions were fragmented using the LIFT mode and the resultant MS/MS spectra was screened for possible peptides using MASCOT (http://www.matrixscience.com/) and de novo sequencing approaches (manual assignment of mass differences). Ions not identified as peptides were submitted as $[M+Na]^+$ and with a mass accuracy of ±2 Da to GlycoMod (http://us.expasy.org/tools/glycomod) to identify possible N-glycan structures (phosphate, sulphate modifications and presence of sialic acids excluded).

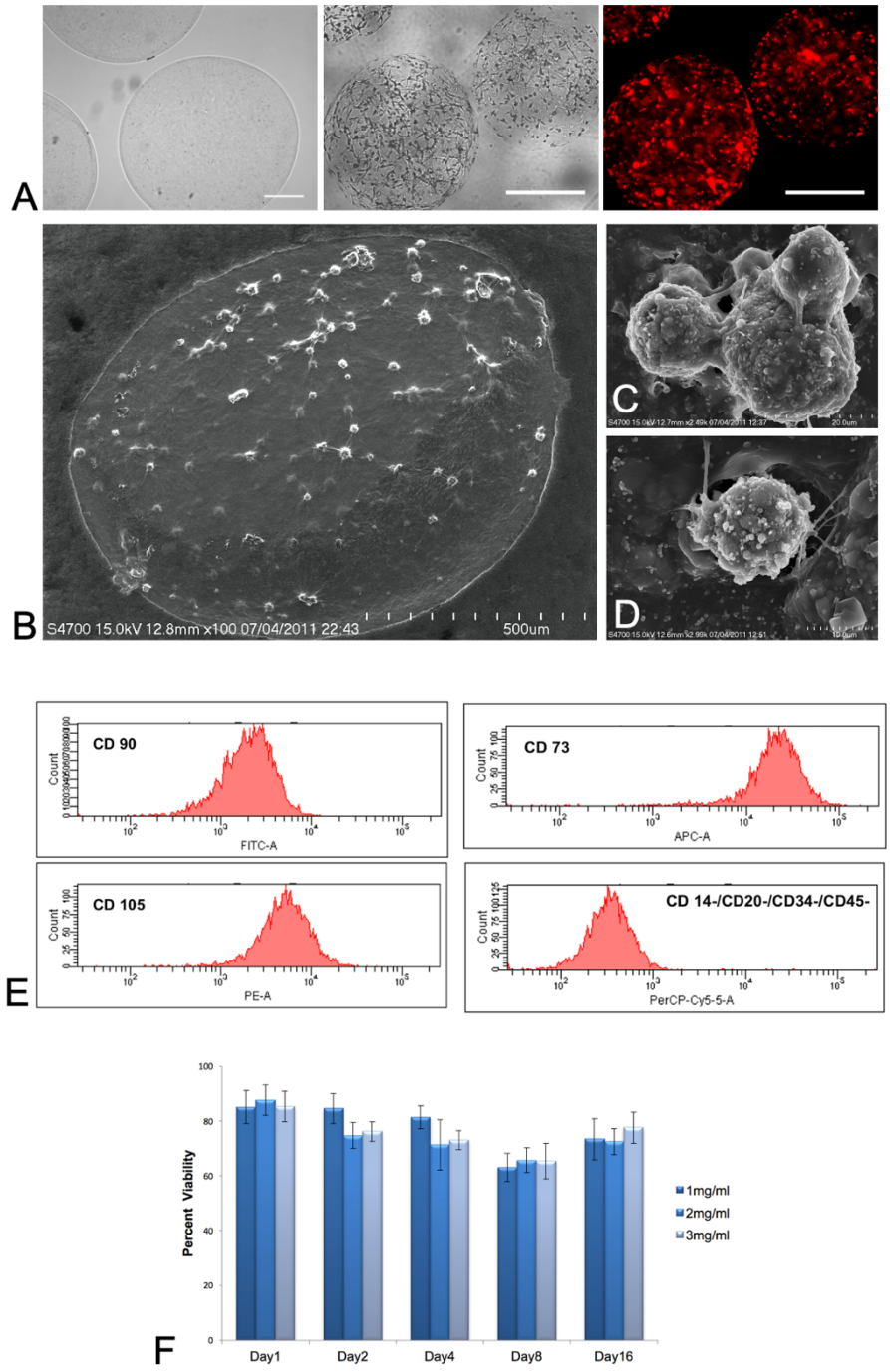

Fig. S1: (A) Microgels unseeded (left); scale bar 200μm, hMSC embedded (center) and PkH-26 labelled hMSCs (right) embedded in microgels after 48 h in vitro (scale bar 500μm).**(B)** SEM micrographs showing topographical appearance of a hMSC seeded microgel with **(C)** cell-cell and **(D)** cell-matrix interaction **(E)** Flow cytometry analysis showing retention of phenotypic human mesenchymal stem cell surface markers 14 days post-seeding on microgels. **(F)** Over 80% cell viability observed for 16 days in all the microgel groups (collagen concentrations 1-mg·mL^{-1}, 2-mg·mL^{-1} and 3-mg·mL^{-1}) at 0.8 million cells mL^{-1} cell density. n=6, P <0.05.

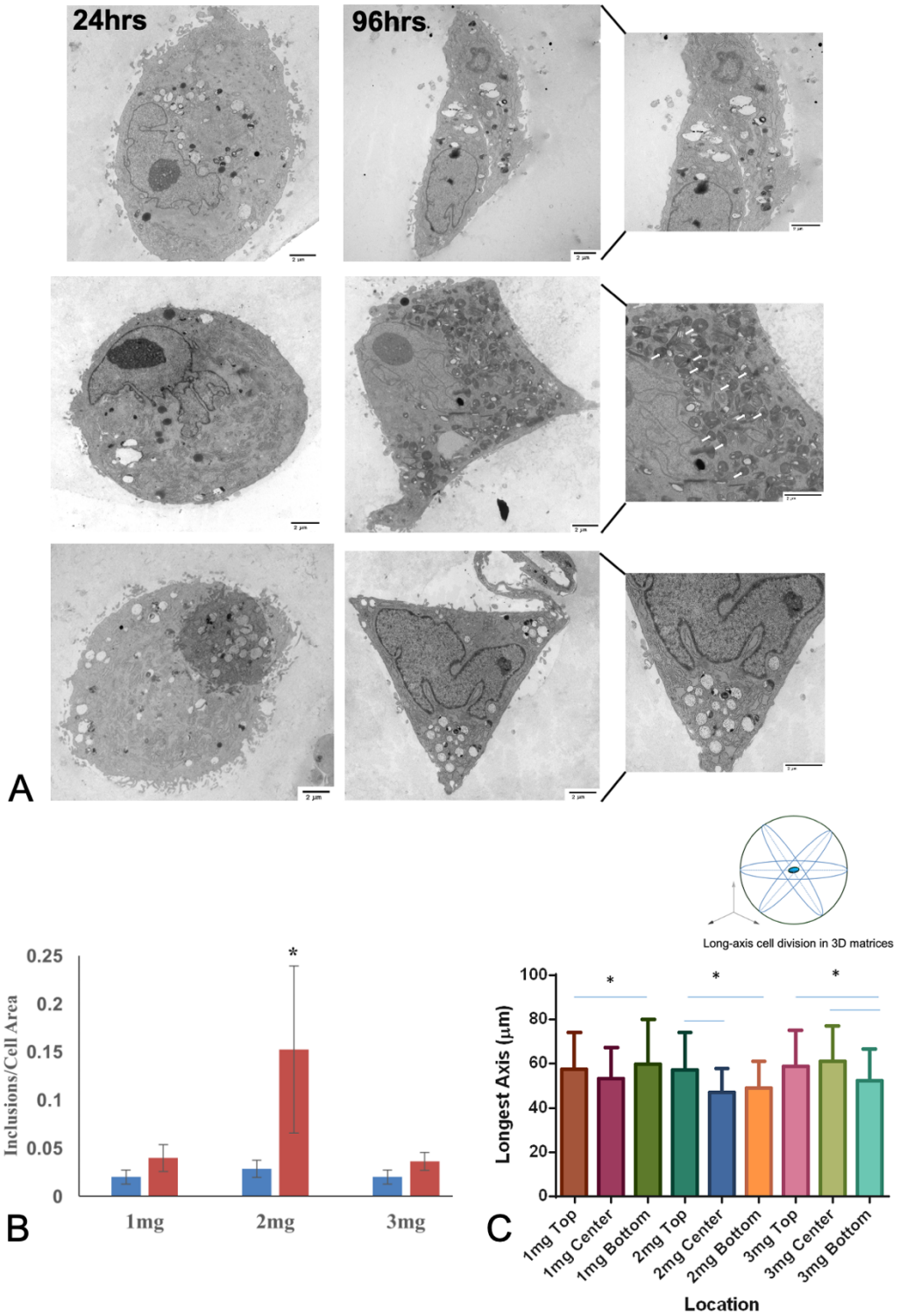

Fig. S2: Preconditioning results in accumulation of intracellular inclusions in hMSCs embedded in microgels. **(A)**TEM micrographs of hMSCs cultured for 96 h containing darkly stained cellular inclusions (indicated with arrows) with distinct cell morphology. Scale bar, 1 µm. **(B)** Quantification of intracellular inclusions in 1, 2 and 3-mg·mL^{-1}microgels (n=5) using FIJI's Trainable WEKA segmentation plugin. **(C)** Differences in hMSC alignment on its longest axis on collagen microgels indicative of cellular anisotropy. * *P* <0.05.

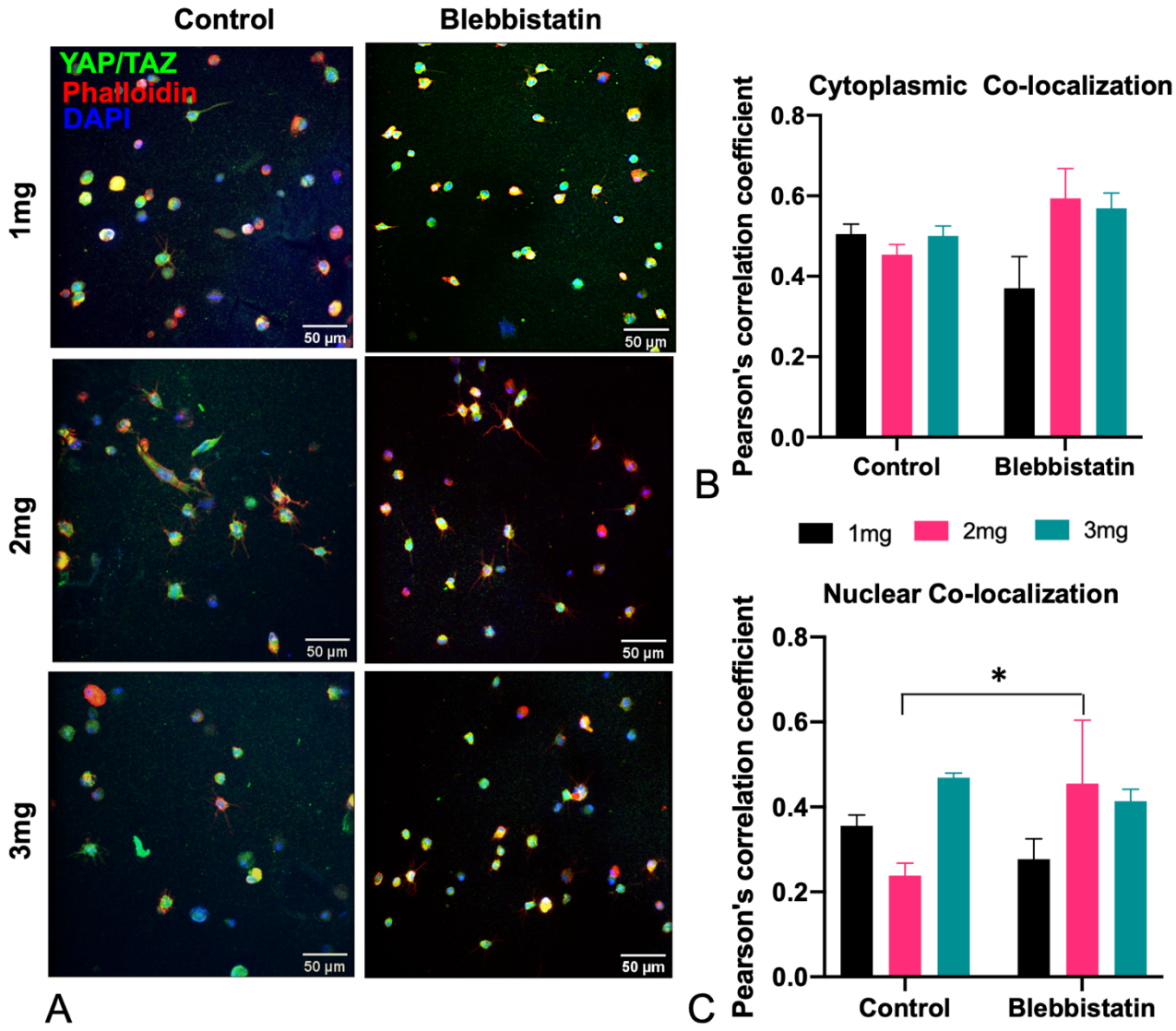

Fig. S3. **(A)** Immunostaining of YAP/TAZ (green), cytoskeleton (red), and nucleus (blue) of human mesenchymal stem cells in 1, 2 and 3-mg·mL^{-1} microgels at 96 h pre-treated with myosin inhibitor blebbistatin. Magnification 20X, Scale bar, 50µm. Quantification of **(B)** cytoplasmic and **(C)** nuclear YAP/TAZ co-localized with the cytoplasm (Phalloidin) or nucleus (DAPI) using Pearson's coefficient for co-localization. Significant increase in nuclear YAP/TAZ co-localization observed in 2-mg·mL^{-1} (n=4) blebbistatin group compared to 2-mg·mL^{-1} control. *P <0.05.

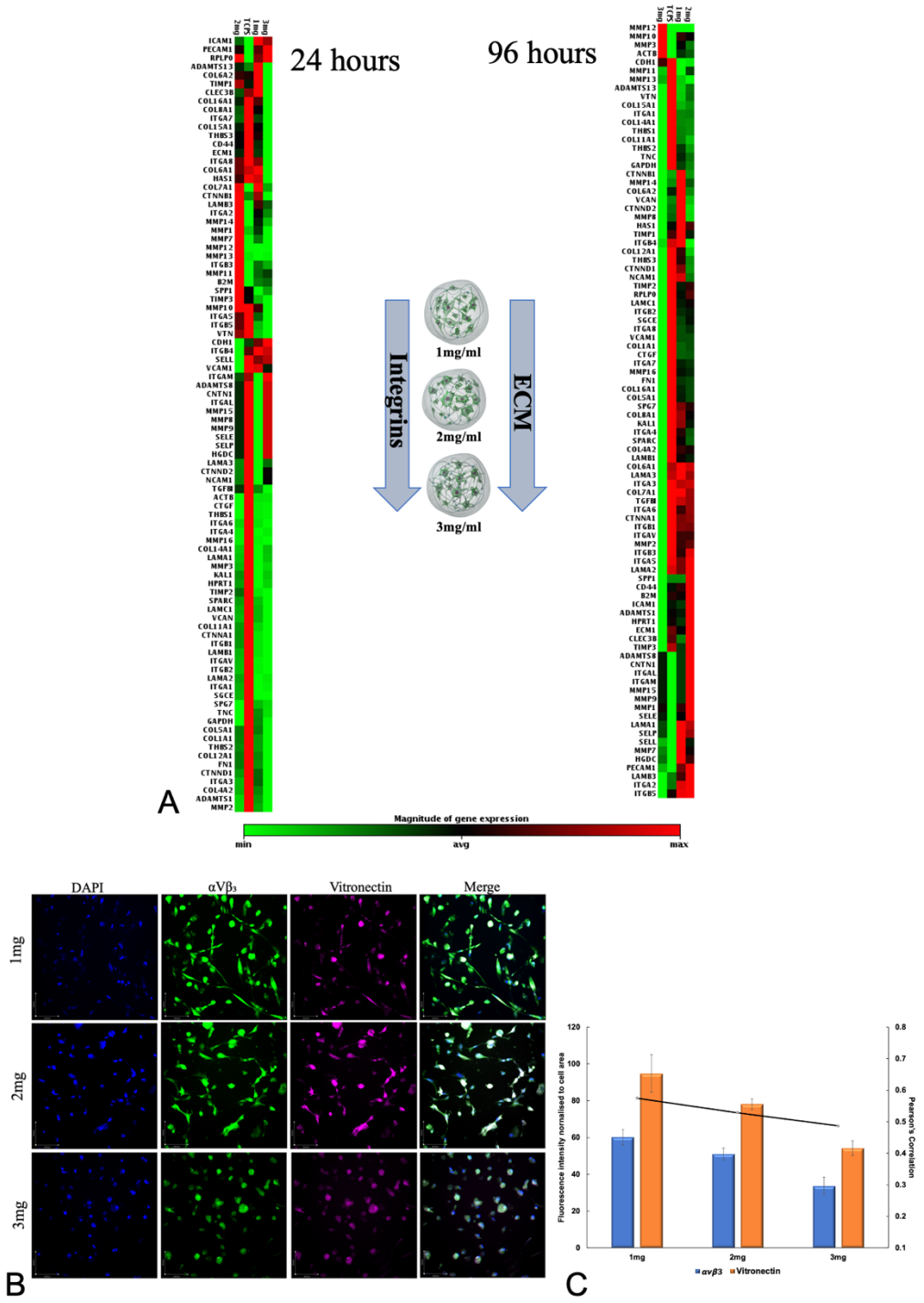

Fig. S4: (A) Heatmap of extracellular matrix and cell adhesion gene markers showing differential fold expression and microgel concentration (1-mg·mL^{-1}, 2-mg·mL^{-1} and 3-mg·mL^{-1}) dependent modulation of genes compared to plastic adherent human mesenchymal stem cells at 24 and 96 h. **(B)** Immunostaining of integrin αVβ$_3$ (green), vitronectin binding domain (magenta), and nucleus (blue) of human mesenchymal stem cells in 1, 2 and 3-mg·mL^{-1} microgels at 96 h. Magnification 20X, Scale bar, 190μm. **(C)** Quantification of protein expression using fluorescence intensity and Pearson's coefficient for co-localization. A linear reduction in expression of integrin αVβ$_3$ and vitronectin is observed with the increase in microgel concentration at 96 h (n=3). *P <0.05.

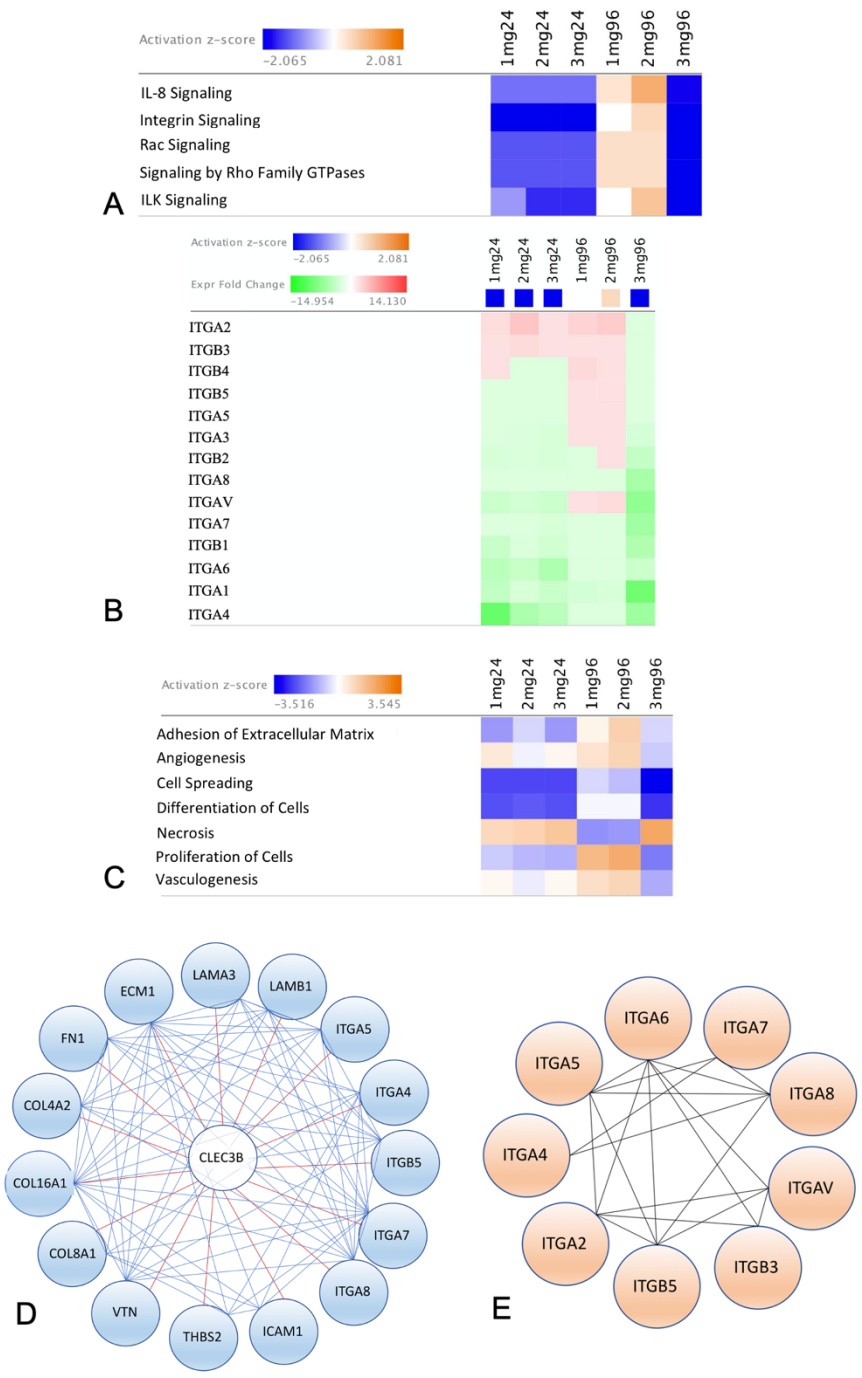

Fig. S5: (A) Heatmap of *z*-scores (indicating activation or inhibition) of canonical pathways Ingenuity Pathway Analysis (IPA) with a threshold of 1.3-fold expression, P <0.05. The dataset represents changes in gene expression at 24 h and 96 h. **(B)** Heatmap of genes in the integrin signalling network expressed as expression fold change **(C)** Heat map displaying *z*-scores of biological functions (IPA). **(D)** Pearson's correlation analysis confirm strong (Pearson's r >0.6) and significant (P <0.05) correlations of gene markers to CLEC3B, identified as the highly enriched node in 2-mg·mL^{-1} microgel condition at 96 h. **(E)** Strong (Pearson's r >0.6) and significant (P <0.05) correlation between integrins in 2-mg·mL^{-1} microgel condition at 96 h.

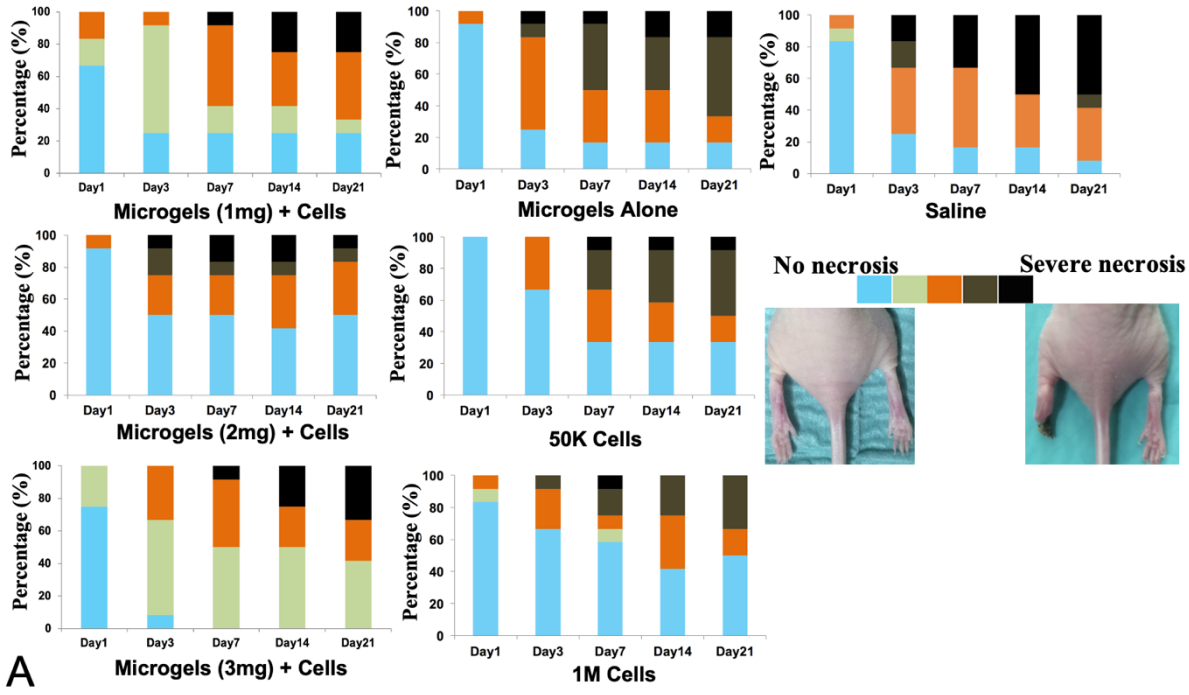

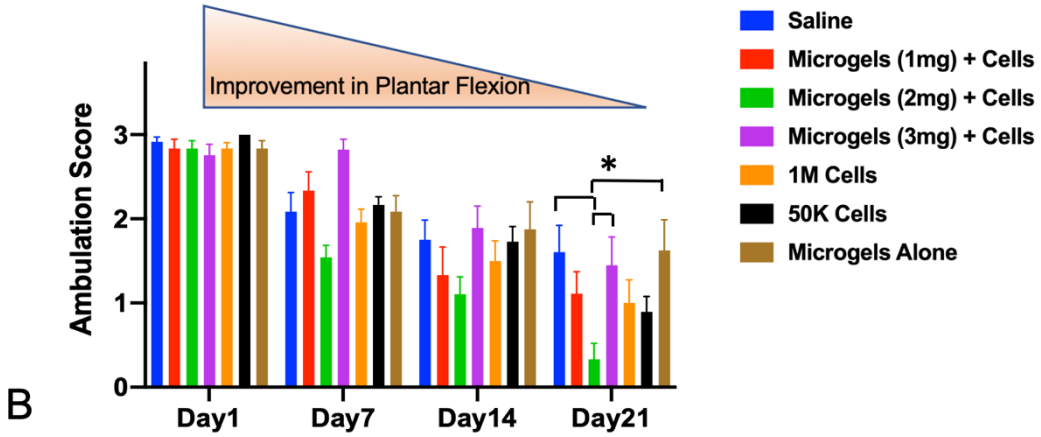

Fig. S6. **(A)** Higher limb salvage in animals treated with hMSC embedded in microgels at a low-cell dose. At day 21 treatment group microgels with hMSCs showed higher limb salvage with 50% (6 out of 12) of the mice protected from tissue damage or necrosis and 15% showing varying degree of moderate to severe necrosis (n=12/group). The color-coded scale is based on a 5-point modified Tarlov scale; 0= Normal, 1= mild redness or cyanosis of toe tips, 2= cyanosis of toes with mild necrosis of toes, 3= moderate necrosis (affecting two or more toes), 4= Severe necrosis affecting the metatarsals, 5= autoamputation of toes/distal limb. **(B)** Significant improvement in ambulation at day 21 in mice treated with hMSC embedded in microgels at a low-cell dose (n=12, *P* <0.05). Hindlimb scoring (index of muscle function); 0= normal, 1= plantar flexion but no flexion of toes, 2= no plantar flexion or dragging and 3= dragging of the foot. A higher score indicates impaired ambulatory function.

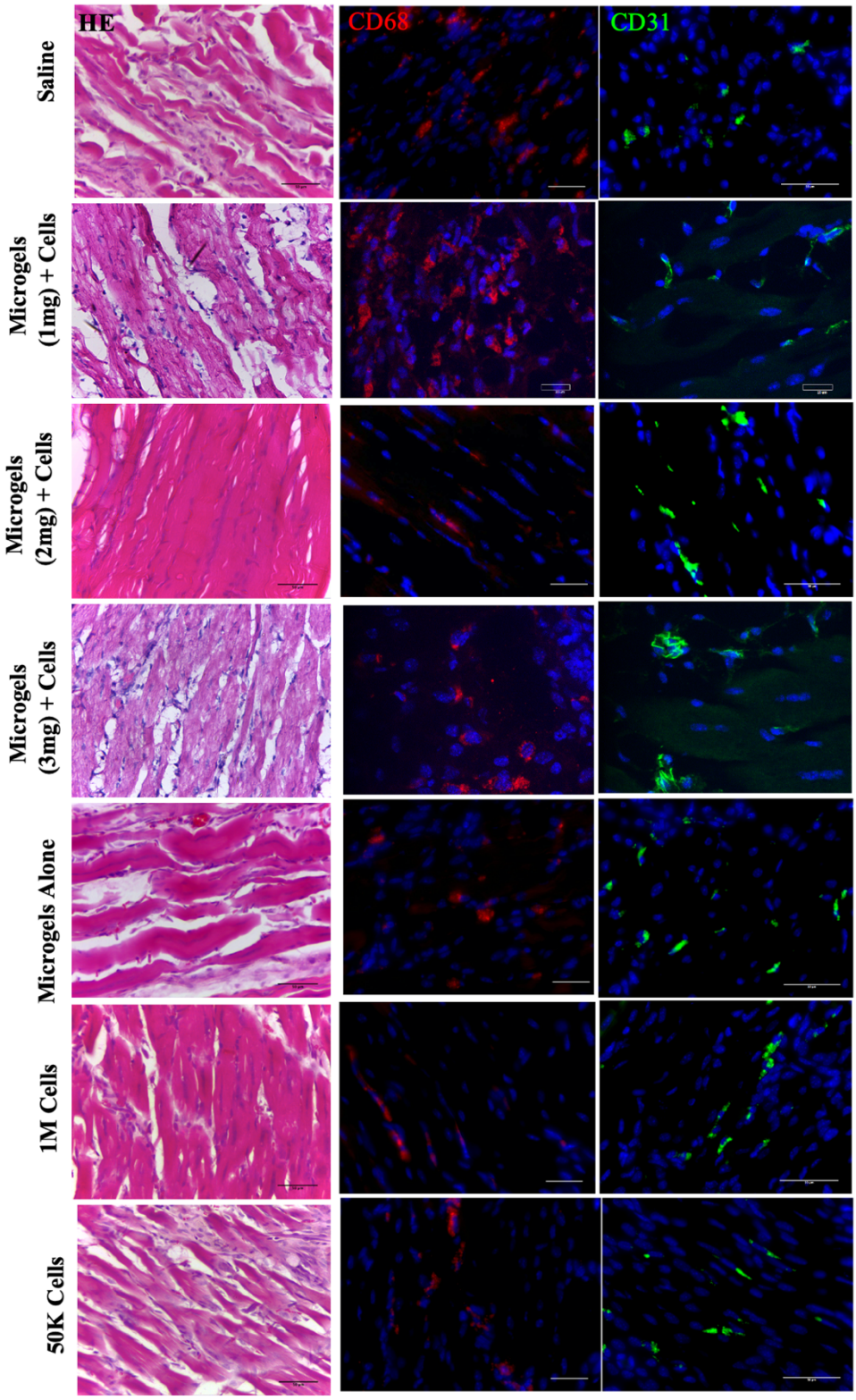

Fig. S7. Immunohistochemical and H&E staining of muscle tissues from treatment groups. CD68 (red) staining for macrophages and CD31 (green) staining for blood vessels.

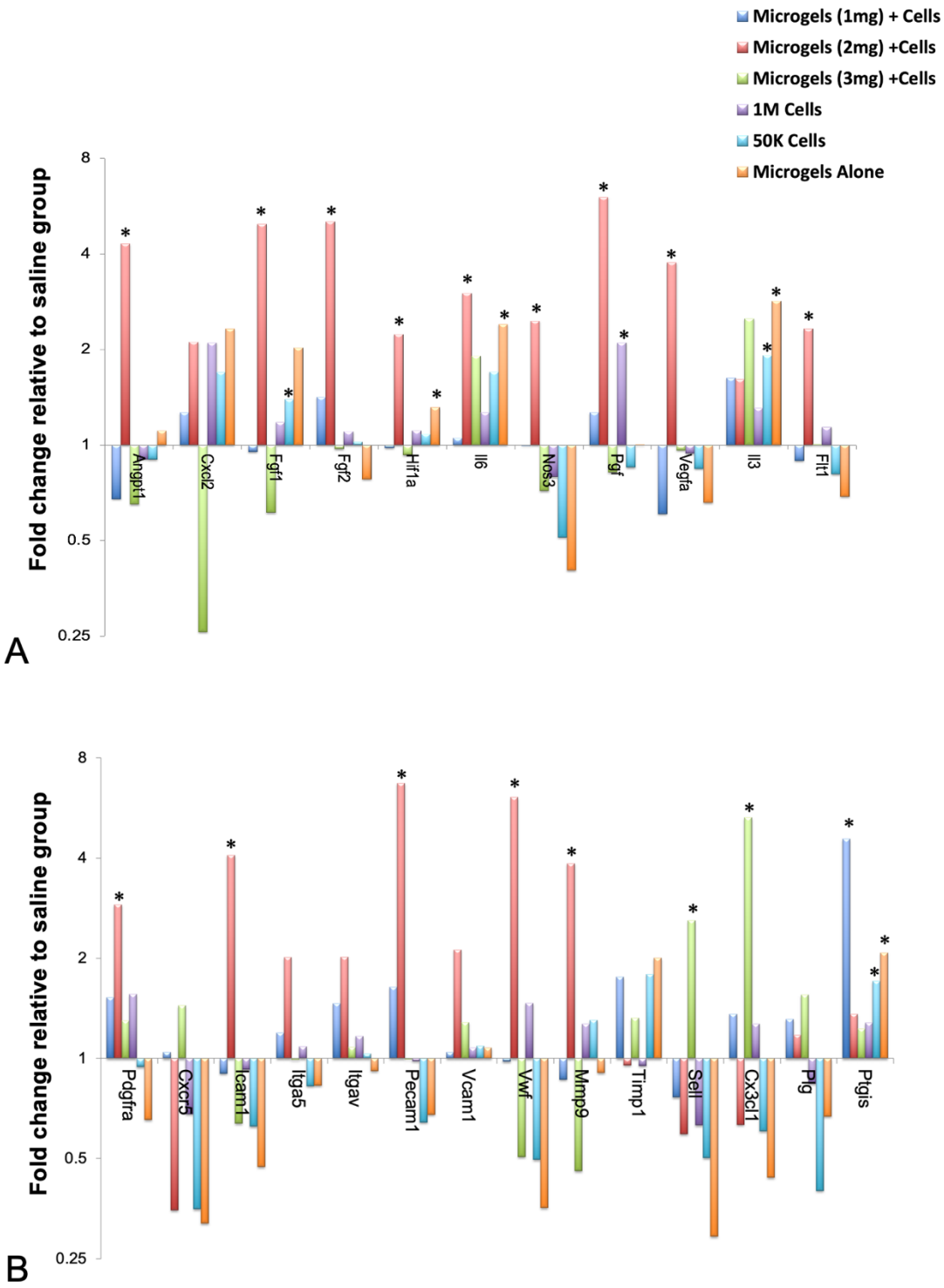

Fig. S8. Significantly high upregulation of genes associated with angiogenesis **(A)** Growth factors and cytokines and **(B)** Extracellular matrix and cell surface markers were observed in mice treated with microgels with hMSCs post-operative at day 21. Statistical significance tested with two-way ANOVA, P <0.05; (n=3/group; n=1 pooled from 4 animals). *P <0.05.

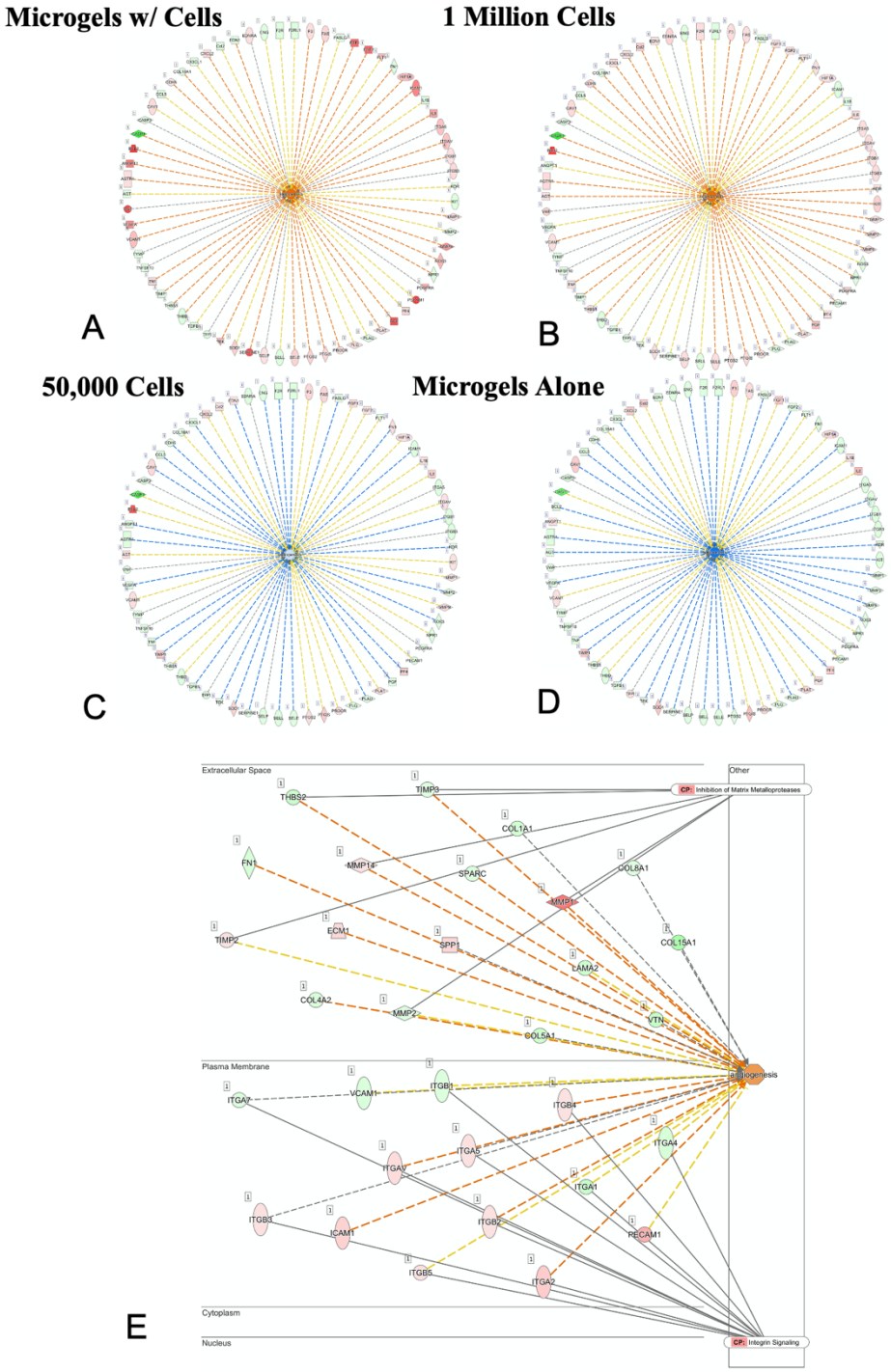

Fig. S9. Ingenuity Pathway Analysis predicted a downstream effect with increased angiogenesis *in vivo* treated with **(A)** microgels with cells (Z-score 2.53) compared to **(B)** 1 million cells (Z-score 2.34), **(C)** 50,000 cells (Z-score -0.24) and **(D)** microgels alone (Z-score -1.78). In microgels with cells group 40 of 68 genes had an expression direction consistent with increased angiogenesis, yielding a Z-score of 2.53. Red symbols indicate increased transcript levels, while green symbol indicate reduced transcript levels. The dotted lines indicate indirect relationships leading to activation (orange) or inhibition (blue). Yellow and grey dotted lines indicate inconsistent relationships and no predicted effects, respectively. **(E)** Molecular network induced by hMSCs embedded in 2-mg·mL^{-1} microgels. Upregulated (red) and downregulated (green) genes resulting in the activation of angiogenesis pathway as revealed by IPA software analysis.

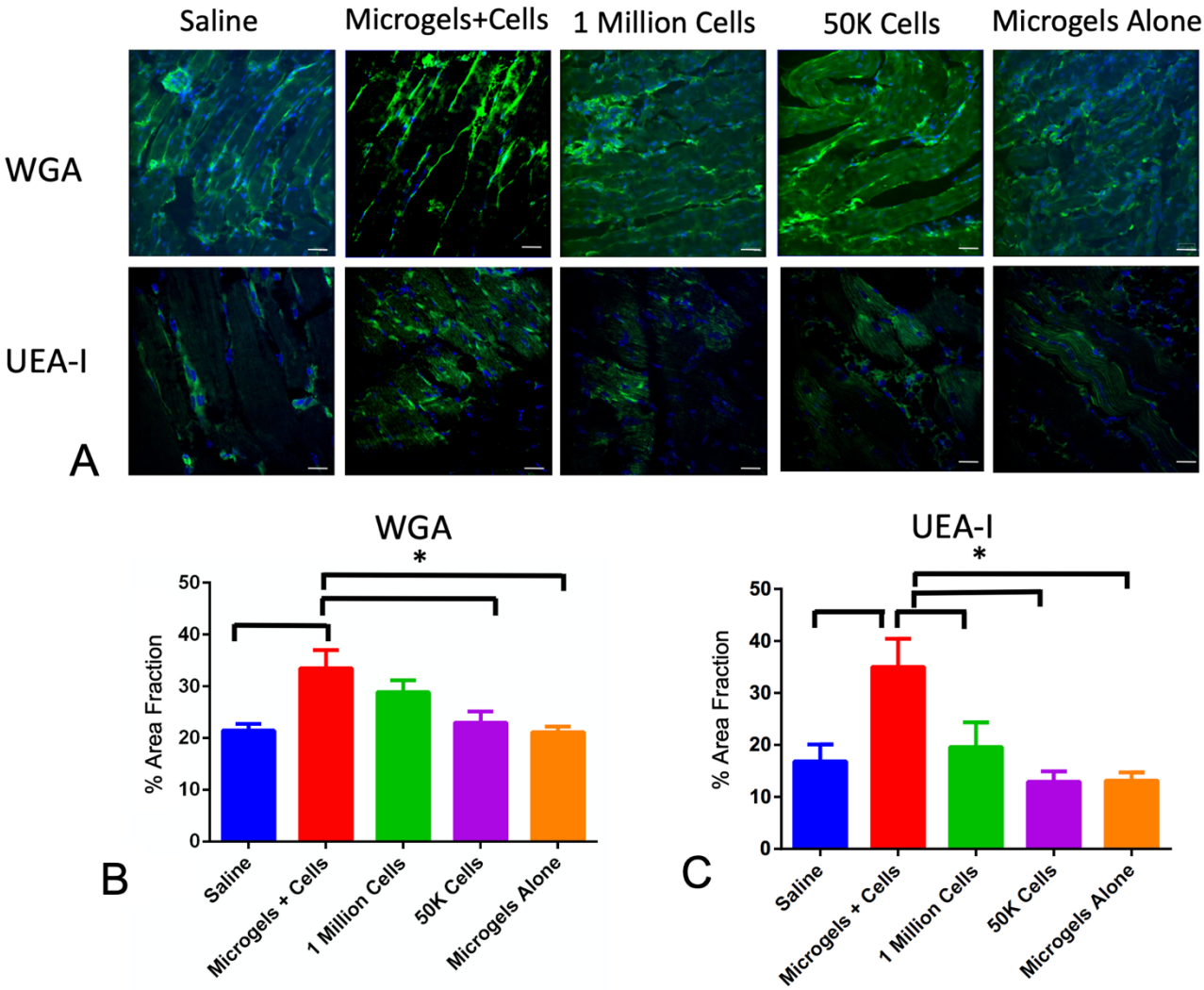

Fig. S10. Higher expression of WGA and UEA-I binding N-linked sugars in the treatment group. **(A)** Lectin immunohistochemical examination of N-linked sugars, N-acetylglucosamine and α-linked fucoses with lectins WGA and UEA-I. Scale bar 50μm. **(B, C)** Percentage area fraction quantification based on the positive expression of the sugars in the upper gastrocnemius muscle tissue. Error bars represent SD *P <0.05 (One-way ANOVA).

Table S1. Integrins and extracellular matrix associated genes quantified using real-time PCR arrays at 24 h.

Refseq	Fold Change	1mg	2mg	3mg	*P* value		
NM_006988	ADAMTS1	-3.6619	-4.7941	-5.6452	0.00011	0.000028	0.000015
NM_139025	ADAMTS13	-1.03	-1.6833	-2.1391	0.914939	0.187613	0.015388
NM_080629	COL11A1	-2.9267	-3.0271	-2.8357	0.000435	0.002107	0.00037
NM_004370	COL12A1	-3.0369	-2.7984	-5.6452	0.000002	0.000003	0.000001
NM_021110	COL14A1	-2.3993	-2.0064	-2.2716	0.011728	0.016806	0.012408
NM_001855	COL15A1	2.8364	-1.3237	-1.4746	0.266421	0.014181	0.013105
NM_001856	COL16A1	-1.4941	-1.9336	-2.6704	0.039006	0.014965	0.006407
NM_000088	COL1A1	-2.3608	-2.0344	-2.8554	0.026649	0.035922	0.013371
NM_001846	COL4A2	-2.6195	-3.1556	-4.3581	0.000401	0.000228	0.000127
NM_000093	COL5A1	-2.7881	-2.6474	-4.1517	0.002718	0.002363	0.000565
NM_001850	COL8A1	-1.8352	-1.8208	-2.23	0.005885	0.000295	0.000022
NM_001901	CTGF	-23.6855	-80.5191	-32.53	0.001326	0.001174	0.001262
NM_001903	CTNNA1	-2.2751	-2.058	-1.8408	0.029556	0.05451	0.028189
NM_001331	CTNND1	-2.0222	-2.4873	-2.8031	0.008589	0.005667	0.001418
NM_002026	FN1	-2.6993	-2.3208	-3.8203	0.010269	0.013668	0.004137
NM_000201	ICAM1	14.1304	5.1292	11.7368	0	0.000016	0
NM_181501	ITGA1	-3.9612	-2.587	-3.4992	0.000013	0.000014	0.000008
NM_002203	ITGA2	2.3306	4.0617	2.0368	0.053691	0.009823	0.004228
NM_002204	ITGA3	-2.0457	-2.3261	-2.5263	0.001073	0.000115	0.000023
NM_000885	ITGA4	-9.9585	-5.4943	-4.4806	0.004433	0.005348	0.005646
NM_000210	ITGA6	-4.375	-3.701	-5.2916	0.000032	0.000036	0.000025
NM_002206	ITGA7	-1.8999	-2.111	-2.5031	0.020846	0.015382	0.00258
NM_002210	ITGAV	-3.3853	-2.8904	-3.3105	0.005408	0.009179	0.00483
NM_002211	ITGB1	-3.6619	-2.4249	-3.0392	0.00001	0.000001	0.000014
NM_000211	ITGB2	-2.5478	-2.375	-2.538	0.004429	0.007681	0.003755
NM_000212	ITGB3	1.4182	2.5293	1.4773	0.051549	0.002152	0.006774
NM_000216	ANOS1	-7.3748	-3.701	-4.9486	0.000168	0.000253	0.000187
NM_005559	LAMA1	-6.2446	-6.4588	-5.0177	0.000031	0.00002	0.000001
NM_000426	LAMA2	-3.3079	-3.0623	-4.7252	0.002153	0.000152	0.000072
NM_000227	LAMA3	-6.6928	-5.7408	-2.4915	0.003105	0.012723	0.011063
NM_002291	LAMB1	-2.8665	-2.4193	-2.8953	0.027368	0.040627	0.024394
NM_000228	LAMB3	1.7951	2.6064	1.598	0.028058	0.001556	0.000013
NM_002293	LAMC1	-2.9813	-2.9375	-3.6059	0.001454	0.001681	0.000757
NM_002421	MMP1	1.7541	2.6004	1.1431	0.009561	0	0.476348
NM_002425	MMP10	-1.5255	-1.6755	-2.0098	0.010072	0.170092	0.002702
NM_005940	MMP11	1.867	3.9233	2.4447	0.068653	0.022442	0.006527
NM_002427	MMP13	1.3232	3.3529	1.1944	0.321517	0.000702	0.552008
NM_005941	MMP16	-3.7216	-3.5176	-2.9493	0.003553	0.003844	0.003728
NM_002423	MMP7	1.6595	3.1794	1.1944	0.125333	0.019935	0.552008
NM_000615	NCAM1	-4.3649	-1.1958	-3.4911	0.000178	0.965691	0.007046
NM_000442	PECAM1	5.9686	6.5074	8.035	0	0.003749	0.000007
NM_003119	SPG7	-1.7727	-2.058	-1.5337	0.030174	0.019686	0.021442
NM_000358	TGFBI	-2.3122	-1.8124	-2.4234	0.000312	0.000524	0.000622
NM_003246	THBS1	-29.4311	-94.0002	-30.1419	0.000001	0	0.000001
NM_003247	THBS2	-2.2438	-1.9742	-2.4403	0.002872	0.002641	0.000612
NM_007112	THBS3	-1.4005	-1.8293	-2.298	0.000969	0.009572	0.00025
NM_003255	TIMP2	-2.656	-1.9879	-2.4067	0.001778	0.008252	0.001295
NM_000362	TIMP3	-1.8868	1.6534	-2.7518	0.028095	0.071822	0.008229
NM_002160	TNC	-2.416	-3.9393	-3.3644	0.00289	0.000941	0.001179

NM_001078	VCAM1	-1.1167	-6.733	-1.7577	0.018539	0	0.000067
NM_004385	VCAN	-4.5397	-4.3307	-9.3202	0.000103	0.000115	0.000095
NM_000638	VTN	-3.0864	-1.3055	-2.298	0.000318	0.015178	0.000148

Table S2. Integrins and extracellular matrix associated genes quantified using real-time PCR arrays at 96 h.

Refseq	Fold Change	1mg	2mg	3mg	*P* value		
NM_006988	ADAMTS1	1.4313	2.0404	-1.3827	0.291948	0.092411	0.261684
NM_139025	ADAMTS13	-4.5714	-2.5336	-15.0062	0.006557	0.018146	0.002676
NM_003278	CLEC3B	-3.0794	2.6187	-2.3416	0.491895	0.00584	0.043711
NM_001843	CNTN1	-2.1033	-2.1652	-1.9108	0.224198	0.268665	0.263192
NM_080629	COL11A1	-30.2593	-6.11	-40.6211	0.041776	0.031804	0.019703
NM_004370	COL12A1	-1.6927	-3.8491	-32.9184	0.127129	0.028925	0.009252
NM_021110	COL14A1	-35.736	-68.9674	-22.1232	0.016574	0.010692	0.004751
NM_001855	COL15A1	-5.2029	-3.8669	-30.9276	0.012388	0.017439	0.006435
NM_001856	COL16A1	-1.3622	-2.0249	-13.0939	0.287203	0.081803	0.015623
NM_000088	COL1A1	-1.5397	-2.0016	-12.359	0.187439	0.105892	0.018435
NM_001846	COL4A2	1.031	-1.6638	-8.6188	0.878401	0.259828	0.019736
NM_000093	COL5A1	-1.4267	-2.2056	-7.858	0.340562	0.195862	0.03415
NM_001848	COL6A1	2.2253	1.612	-2.2153	0.079158	0.36556	0.158815
NM_001849	COL6A2	1.7022	1.4065	-2.6223	0.281298	0.421352	0.152427
NM_000094	COL7A1	1.06	-1.531	-7.4858	0.846218	0.316742	0.007285
NM_001850	COL8A1	1.0454	-1.5346	-10.1318	0.849889	0.132168	0.003106
NM_001901	CTGF	-2.0839	-2.1954	-6.5318	0.059351	0.054333	0.012905
NM_001331	CTNND1	-1.0541	-1.4418	-3.2735	0.877398	0.526991	0.002471
NM_004425	ECM1	1.7703	2.7362	-2.0527	0.225514	0.246841	0.090306
NM_002026	FN1	-1.4333	-1.6871	-7.5903	0.276179	0.187048	0.037213
NM_000201	ICAM1	2.0667	3.0784	1.3279	0.050834	0.067378	0.539919
NM_181501	ITGA1	-2.8205	-2.5336	-9.4971	0.026033	0.03104	0.008707
NM_002203	ITGA2	2.9981	3.5707	-1.0576	0.036151	0.02698	0.915943
NM_002204	ITGA3	1.0773	1.3586	-2.6162	0.874485	0.292609	0.046838
NM_000885	ITGA4	-1.2858	-1.7305	-6.3827	0.28309	0.096872	0.000191
NM_002205	ITGA5	1.6611	2.0383	-1.6789	0.286055	0.024094	0.157791

NM_000210	ITGA6	-1.0135	-1.0603	-3.35	0.974391	0.659283	0.012378
NM_002206	ITGA7	-1.1116	-1.5887	-6.2513	0.912247	0.065609	0.004835
NM_003638	ITGA8	-1.4201	-1.7225	-5.7924	0.244077	0.077203	0.009736
NM_002210	ITGAV	1.436	2.4463	-7.2308	0.526281	0.58429	0.014234
NM_002211	ITGB1	-1.1969	-1.1156	-5.113	0.633716	0.758885	0.082413
NM_000211	ITGB2	-1.0565	1.2076	-3.8749	0.835744	0.647437	0.034589
NM_000212	ITGB3	1.3954	2.003	-2.0574	0.459113	0.036211	0.060875
NM_000213	ITGB4	2.5859	1.0586	-1.5628	0.224846	0.944684	0.303658
NM_002213	ITGB5	1.8474	2.21	-1.2318	0.215782	0.013062	0.490664
NM_000216	ANOS1	1.284	-1.7506	-6.825	0.659121	0.221638	0.060856
NM_005559	LAMA1	2.4072	1.8906	1.194	0.363288	0.491004	0.855663
NM_000426	LAMA2	-1.6051	-2.1954	-15.357	0.469286	0.164689	0.06037
NM_000227	LAMA3	3.0469	1.5788	-2.0151	0.301858	0.175204	0.115915
NM_002291	LAMB1	1.1981	-1.2522	-6.0523	0.801917	0.434265	0.054972
NM_000228	LAMB3	3.2506	2.5707	-1.4717	0.186198	0.15207	0.39836
NM_002293	LAMC1	-1.62	-1.4154	-7.8944	0.106215	0.193932	0.009004
NM_002421	MMP1	9.3223	11.9491	9.0579	0.000272	0.012838	0.000667
NM_002425	MMP10	5.5175	3.4633	5.5245	0.000688	0.0464	0.124706
NM_002426	MMP12	7.2973	5.2011	8714.3504	0.37064	0.374811	0.373899
NM_002427	MMP13	-2.6561	-3.1264	-1.5166	0.072851	0.061098	0.215509
NM_005941	MMP16	-1.3311	-1.3328	-4.4203	0.442529	0.412449	0.059845
NM_004530	MMP2	-1.0565	-1.1234	-2.5388	0.652923	0.504051	0.008733
NM_002422	MMP3	6.0658	4.7201	10.2142	0.059123	0.005099	0.10578
NM_002424	MMP8	-1.8058	-3.1627	-2.4637	0.319593	0.061837	0.10789
NM_000615	NCAM1	1.8974	1.4098	-2.2	0.07635	0.416929	0.050517
NM_000442	PECAM1	3.8478	5.6784	1.9442	0.022118	0.027027	0.058111
NM_003919	SGCE	-2.0648	-1.4023	-5.4673	0.175387	0.419069	0.038389
NM_003118	SPARC	-1.5648	-1.531	-4.2698	0.196233	0.409777	0.037024
NM_000582	SPP1	1.4413	2.9735	1.0371	0.111107	0.040731	0.786489

NM_000358	TGFBI	1.8799	2.3546	-1.581	0.486057	0.199921	0.257902
NM_003246	THBS1	-2.9268	-2.7661	-10.5134	0.026908	0.027556	0.008417
NM_003247	THBS2	-1.5903	-2.3804	-11.1128	0.185701	0.067659	0.010294
NM_007112	THBS3	-1.583	-3.055	-11.1643	0.060015	0.000989	0.000307
NM_003255	TIMP2	-1.0348	1.2853	-3.162	0.767286	0.693697	0.107756
NM_000362	TIMP3	-1.8142	-1.1985	-4.3797	0.24341	0.960682	0.03186
NM_002160	TNC	-1.4135	-1.1929	-8.6988	0.286224	0.898452	0.03333
NM_001078	VCAM1	-1.9761	-1.6072	-10.7343	0.076188	0.300433	0.011799
NM_004385	VCAN	1.3417	-1.3115	-9.9233	0.700811	0.823258	0.183297
NM_000638	VTN	-2.3663	-2.5689	-5.7924	0.222895	0.025737	0.009688

SI References

1. J. I. Kilpatrick, I. Revenko, B. J. Rodriguez, Nanomechanics of cells and biomaterials studied by atomic force microscopy. *Adv. Healthc. Mater.* **4**, 2456–2474 (2015).
2. M. Ahearne, Y. Yang, A. J. El Haj, K. Y. Then, K.-K. Liu, Characterizing the viscoelastic properties of thin hydrogel-based constructs for tissue engineering applications. *J. R. Soc. Interface* **2**, 455–463 (2005).
3. J. Schindelin, *et al.*, Fiji: an open-source platform for biological-image analysis. *Nat. Methods* **9**, 676–682 (2012).
4. D. Thomas, *et al.*, Variability in endogenous perfusion recovery of immunocompromised mouse models of limb ischemia. *Tissue Eng. Part C, Methods* **22**, 370–381 (2016).
5. Y. Garcia, A. Breen, K. Burugapalli, P. Dockery, A. Pandit, Stereological methods to assess tissue response for tissue-engineered scaffolds. *Biomaterials* **28**, 175–186 (2007).
6. D. Thomas, *et al.*, A shape-controlled tuneable microgel platform to modulate angiogenic paracrine responses in stem cells. *Biomaterials* **35**, 8757–8766 (2014).
7. B. C. Dash, *et al.*, An injectable elastin-based gene delivery platform for dose-dependent modulation of angiogenesis and inflammation for critical limb ischemia. *Biomaterials* **65**, 126–139 (2015).
8. P. Dockery, J. Fraher, The quantification of vascular beds: A stereological approach. *Exp. Mol. Pathol.* **82**, 110–120 (2007).
9. A. Breen, G. Mc Redmond, P. Dockery, T. O'Brien, A. Pandit, Assessment of wound healing in the alloxan-induced diabetic rabbit ear model. *J. Invest. Surg.* **21**, 261–269 (2008).
10. T. M. Mayhew, The new stereological methods for interpreting functional morphology from slices of cells and organs. *Exp. Physiol.* **76**, 639–665 (1991).
11. M. W. Pfaffl, G. W. Horgan, L. Dempfle, Relative expression software tool (REST) for group-wise comparison and statistical analysis of relative expression results in real-time PCR. *Nucleic Acids Res.* **30**, e36 (2002).
12. J. Yang, R. M. Caprioli, Matrix sublimation/recrystallization for imaging proteins by mass spectrometry at high spatial resolution. *Anal. Chem.* **83**, 5728–5734 (2011).